American Mineralogist, Volume 97, pages 38–51, 2012

The mechanism of thermal decomposition of dolomite: New insights from 2D-XRD and TEM analyses

Carlos Rodriguez-Navarro,* Krzysztof Kudlacz, and Encarnacion Ruiz-Agudo

Department Mineralogía y Petrología, Universidad de Granada, Fuentenueva s/n, 18071 Granada, Spain

Abstract

Despite being studied for more than one century, no consensus exists regarding the ultimate mechanism(s) of the thermal decomposition of dolomite [($CaMg(CO_3)_2$]. To shed light on such a reaction, dolomite single crystals were calcined in air between 500 and 1000 °C, and in situ, in a TEM (high vacuum), following irradiation with the electron beam. In situ TEM shows that the decomposition involves the initial formation of a face centered cubic mixed oxide ($Ca_{0.5}Mg_{0.5}O$) with reactant/product orientation relationships $[001]_{dolomite}//<111>_{oxide}$, $<\bar{4}41>_{dolomite}//<100>_{oxide}$, $\{11\bar{2}0\}_{dolomite}//\{110\}_{oxide}$, $\{11\bar{2}8\}_{dolomite}//\{110\}_{oxide}$ and $\{10\bar{1}4\}_{dolomite}\wedge\{100\}_{oxide}$~12°. This phase undergoes de-mixing into oriented crystals of Mg-poor CaO and Ca-poor MgO solid solutions upon long-term e-beam exposure. Ex situ TEM, XRD, 2D-XRD, and FESEM analyses show the formation of porous pseudomorphs made up of oxide nanocrystals with similar parent/product orientation relationships, but with limited Ca/Mg substitution (up to ~9–11%) due to de-mixing (spinodal decomposition) of the metastable (Ca,Mg)O precursor. High ion diffusivity at $T > 500$ °C (ex situ experiments) favors the formation of pure CaO and MgO crystals during coarsening via oriented aggregation and sintering. These results show that the thermal decomposition of dolomite is topotactic and independent of pCO_2. Formation of Mg-calcite nanocrystals (up to ~8 mol% Mg) during the so-called "half decomposition" is observed at 650–750 °C. This transient phase formed topotactically following the reaction of CaO nanocystals (solid solution with ~9 mol% Mg) with CO_2 present in the air and/or released upon further dolomite decomposition. With increasing T, Mg-calcite transformed into calcite, which underwent decomposition following the known topotactic relationship: $\{10\bar{1}4\}_{calcite}//\{110\}_{CaO}$ and $<\bar{4}41>_{calcite}//<110>_{CaO}$. These observations solve the long standing controversy on the mechanism of the "two-stage" decomposition of dolomite, which assumed the direct formation of calcite during the so-called "half decomposition."

Keywords: Dolomite, lime, periclase, thermal decomposition, half decomposition, (Ca,Mg)O mixed oxide, 2D-XRD, TEM-SAED, topotactic

Introduction

The thermally induced decomposition of dolomite [$CaMg(CO_3)_2$] is of geological significance both at a local scale during meteorite impact and pyrometamorphism (Grapes 2006) and at a large scale in subduction zones and high-grade metamorphism (Best 1982). Dolomite thermal decomposition is also of technological importance in the construction, ceramics, glass, iron, and steel industry, in pharmacy, as a source of CaO and MgO, and as a gas scrubber for pollutant gases (Siegel et al. 1978; De Aza et al. 2002; Cultrone et al. 2008). Due to its scientific and technological importance, numerous studies on the thermal decomposition of dolomite have been performed over the last 100 years (Galwey and Brown 1999; De Aza et al. 2002; Galai et al. 2007, and references therein). However, the mechanism(s) of this reaction are still poorly understood.

Depending on T and pCO_2, dolomite decomposition is reported to follow two different paths: (1) the so-called "one-step" ("one-stage") or "full-decomposition", and (2) the "two-step" ("two-stage") or "half-decomposition" routes. At low pCO_2 [i.e., pCO_2 below 0.016–0.267 bar at 685–700 °C (Bandi and Krapf 1976; Powell and Searcy 1978)] dolomite undergoes a "one-step" decomposition according to the reaction $CaMg(CO_3)_2 \rightarrow CaO + MgO + 2CO_2$ (Britton et al. 1951; Haul and Markus 1952; Powell and Searcy 1978; Engler et al. 1989). At high pCO_2, the decomposition path is commonly represented by a "two-step" reaction, (1) $CaMg(CO_3)_2 \rightarrow CaCO_3 + MgO + CO_2$ (i.e., "half decomposition") and (2) $CaCO_3 \rightarrow CaO + CO_2$, which proceed sequentially at a T that depends on the experimental conditions (pCO_2, crystal size, sample mass, and heating rate) (Lange and Roesky 1964; Milodowski et al. 1989; De Aza et al. 2002). Whereas the mechanism of decomposition of $CaCO_3$ according to reaction 2 is now well understood (Rodriguez-Navarro et al. 2009), the so-called "half decomposition" or "half calcination" of dolomite (reaction 1) has been, and still is a matter of strong controversy. Several, mutually excluding mechanistic models have been proposed for such a reaction. (1) Dissociation into the pure carbonates $CaMg(CO_3)_2 \rightarrow CaCO_3 + MgCO_3$ and successive decomposition of $MgCO_3$ into MgO and CO_2 (Samtani et al. 2001). (2) A formation of a "mixed crystal" between calcite and magnesite following the reaction $CaMg(CO_3)_2 \rightarrow CaCO_3(1-n)MgCO_3 + nMgO + nCO_2$, where n increases from 0 to 1 with time (Hashimoto et al. 1980)

* E-mail: carlosrn@ugr.es

or via a metastable solid-solution precursor according to the reaction $CaMg(CO_3)_2 \rightarrow (1 - x)CaCO_3(1 - y)MgO + xCaCO_3 + yMgO + CO_2$ (Beruto et al. 2003b). (3) The direct formation of MgO and CaO, followed by the immediate recarbonation of CaO to yield $CaCO_3$ (Britton et al. 1951; Lange and Roesky 1964; Wiedemann and Bayer 1987). (4) The direct formation of calcite and periclase (MgO) according to reaction 1. This latter model appears to be the most widely accepted mechanism for the "half decomposition" of dolomite (Wilsdorf and Haul 1951; Haul and Markus 1952; Haul and Raal 1955; Bandi and Krapf 1976; Siegel et al. 1978; Engler et al. 1989; De Aza et al. 2002; Galai et al. 2007).

Wilsdorf and Haul (1951) concluded that the transformation between dolomite and calcite was topotatic. Other authors such as Dasgupta (1967), Singh Dev (1972), and Hashimoto et al. (1980) also suggested that the thermal decomposition of dolomite was topotactic. However, no consensus exists regarding the parent/product orientation relationships or the actual mechanism(s) of such a transformation.

In an effort to shed light on the ultimate mechanism of dolomite thermal decomposition, we studied the chemical-microstructural features of dolomite single crystals thermally decomposed in air in a range of T (500–1000 °C) and different heating conditions (from flash decomposition to slow heating/long soaking time experiments), as well as in high vacuum [in situ decomposition in the transmission electron microscope (TEM)].

Materials and methods

Dolomite crystals and their thermal decomposition

High-purity, optical quality dolomite crystals from Eugui, Pamplona (Spain), were used thoroughout. The powder X-ray diffraction (XRD) pattern of Eugui dolomite showed the presence of strong order (or superstructure) reflections (Lippmann 1973) confirming its crystalline perfection. Crystals were cleaved using a blade to obtain millimeter-sized (ca. 3 × 2 × 1 mm) fragments, placed in ceramic crucibles (two to three crystals, total mass ca. 170 mg, per cylindrically shaped, 1.5 cm diameter × 5 cm tall crucible) and calcined in an air-ventilated electric furnace (Select-Horn, Selecta). Errors in recorded T were on the order of ±5 °C in the working T interval. Two different calcinations runs, here denoted run A and run B, were performed. At least three replicates per run were done. During run A, the oven was heated once the samples were placed inside from 25 °C up to the target T at a rate of 2 °C/min. Once each target T was reached, a retention (soaking) time of 30 min was used before reaching the next target T (at 50 °C increments from 500 up to 1000 °C). In run B, ("flash decomposition") the oven was pre-heated from 25 up to the 400 °C, and samples were placed inside the oven for one hour. This procedure was applied to release strain and avoid the decrepitation of crystals during the following step of the heating procedure, leading to their jumping out of the crucible. XRD and TEM analysis of crystals heated at 400 °C showed no sign of decomposition. Subsequently, the oven was heated to the target T (500–800 °C at 50 °C increments, and at 900 °C). At each target T, samples were separately placed in the oven during 15 min. In the case of samples subjected to flash calcination at 650 and 700 °C, two additional runs with a soaking time of 5 and 10 min were performed. This was done to study in detail the formation of $CaCO_3$ during the two-stage decomposition of dolomite. After soaking at each target T in both runs A and B, samples were collected, cooled at room T, weighed, and introduced in tightly capped vials under dry N_2 atmosphere before further analysis.

Thermogravimetric (TG) analyses were performed in flowing (100 cm^3/min) air atmosphere on a Shimadzu TGA-50H analyzer equipped with a Mettler-Toledo AX26 Delta Range microbalance. For each TG run, the temperature was risen from 25 up to 950 °C at different heating rates, β, of 2, 5, 10, and 15 °C/min. In each measurement a single crystal (ca. 2 × 2 × 1 mm in size) of ~10 mg was placed into a Pt crucible, and weight loss data were collected at regular time intervals. Such a small sample size was selected to minimize mass effects associated with an increase in the partial pressure of CO_2 around and within the reacting crystal.

Mineralogical and textural analysis by XRD and 2D-XRD

Analysis of phase evolution with calcination T was performed using a Philips PW-1710 diffractometer with Cu$K\alpha$ radiation (λ = 1.5405 Å). Data were collected from 20 to 70 °2θ at a counting rate of 0.03 °2θ s^{-1}. Thermally treated dolomite samples were grinded in an agate mortar and placed in zero-background silicon sample holders for powder XRD analysis. Additionally, non-grinded calcined dolomite single crystals (pseudomorphs) were placed in the diffractometer chamber with their $\{10\bar{1}4\}$ cleavage plane parallel to the zero-background silicon sample holder and XRD patterns were collected. The evolution of CaO and MgO crystallite size with T was calculated from peak-broadening analysis (Rodriguez-Navarro et al. 2009).

Pole figures describing the 3D orientation relationships between dolomite pseudomorphs and product crystals, i.e., lime and periclase (and $CaCO_3$), were determined using an X-ray single-crystal diffractometer equipped with an area detector (D8 SMART APEX, Bruker) following the 2D-XRD analytical procedure described in Rodriguez-Navarro et al. (2009).

Electron microscopy analyses

Analysis of the shape, size, and microstructure of reactant and product phases was performed by means of field emission scanning electron microscopy (FESEM) using a Leo Gemini 1530 and TEM using a Philips CM20, operated at a 200 kV acceleration voltage. For FESEM analysis, single crystals heated at different T were placed onto carbon-coated sticky stubs before carbon coating. Prior to TEM observations samples were gently ground in an agate mortar and dispersed in ethanol, placed in ultrasound for 60 s, and finally deposited on Formbar-coated or carbon-coated copper grids. TEM observations were performed using a 40 µm objective aperture. SAED patterns were collected using a 10 µm aperture, which allowed collection of diffraction data from a circular area of 0.5 µm in diameter. In situ decomposition of dolomite crystals (about 2–5 µm in size) due to electron beam damage was also observed in the TEM (i.e., high-vacuum conditions). The electron flux was maximized using a large (200 µm) condenser aperture and a focused beam spot size of ~200 nm, thus providing an estimated electron flux of ca. 50–70 A/cm^2. Under these conditions, full conversion was achieved after ~1–5 min exposure.

Results and discussion

Calcination and weight-loss evolution

Thermal decomposition of dolomite single crystals in the electric furnace (runs A and B) resulted in pseudomorphs that fully preserved the external shape of the $\{10\bar{1}4\}$ rhombohedron. The core of partially decomposed pseudomorphs was a transparent rhombohedron surrounded by a brownish external shell. These observations suggest that there is a crystallographic control in the advancement of the reactant-product interface, through which CO_2 diffuses outside while the reaction progresses from the surface toward the core. In this respect, the reaction progresses identically as in the case of other carbonates such as calcite (Rodriguez-Navarro et al. 2009).

Figure 1 shows weight loss vs. T for the dolomite single crystal calcined at a heating rate of 10 °C/min in the TG. We failed to obtain reliable TG results for crystals heated at 2, 5, and 15 °C/min due to sudden and significant weight losses in the T range 285–500 °C. Such an effect has been associated to decrepitation (McCauley and Johnson 1991). It prevented us from performing a non-isothermal kinetic analysis of the thermal decomposition of dolomite single crystals. Despite these limitations, TG results show that the decomposition of dolomite single crystals in air follows what appears to be a one-stage decomposition route (e.g., Bandi and Krapf 1976). Decomposition starts at ca. 500 °C and initially progressed at a relatively slow rate up to 750 °C when a faster, nearly constant decomposition rate was observed up to the full decomposition (at ~900 °C). However, a two-stage weight loss was typically observed in the decomposition runs performed in the electric furnace under a static air atmosphere

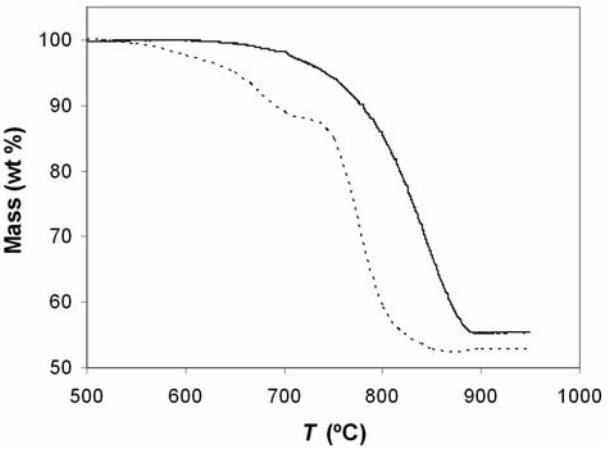

FIGURE 1. Weight loss vs. *T* of dolomite single crystals calcined (in air) in the TG at a heating rate of 10 °C/min (solid line) and in the electric furnace at a heating rate of 2 °C/min (dashed line).

and at an overall heating rate of 2 °C/min (run A) (Fig. 1). The transition between the first and second weight loss events occurred within a short range of *T* (650–750 °C). This latter trend in weight loss is consistent with some studies (using TG, DTA, and in situ XRD) that report a two-stage decomposition in air (Lange and Roesky 1964; Engler et al. 1989). Such a behavior has been observed when pCO_2 is close to the transition between a one-step and a two-step decomposition mechanism (Haul and Markus 1952; Bandi and Krapf 1976; Wiedemann and Bayer 1987). Procedural variables (e.g., static vs. dynamic atmosphere, as well as differences in heating rate and sample mass) appear to account for the differences in weight loss trends between TG and oven experiments (run A). In particular, mass effects account for a self-generated CO_2 atmosphere, which induces a two-stage decomposition process above a critical threshold mass value (Samtani et al. 2001). In any case, we observed that the final weight loss ranged from 44.6–45.6 wt% (TG runs) up to 47.1 wt% (run A). These values approach the theoretical weight loss of pure, stoichiometric dolomite (47.7 wt%) (Powell and Searcy 1978).

Phase evolution with *T*: XRD analyses

Powder XRD analysis of ground dolomite pseudomorphs (run A) showed the presence of dolomite up to 800–850 °C. Up to its full decomposition, dolomite showed strong order reflections (Fig. 2a). This implies that no significant thermally induced disorder in the alternating layers of Ca and Mg occurred prior to decomposition. On the other hand, no reflections corresponding to magnesite were observed. Thus, models assuming the counter-diffusion of Mg and Ca to form Ca-rich and Mg-rich microdomains preceding the collapse of dolomite structure (e.g., Bradley et al. 1953), as well as those assuming the decomposition into two carbonates prior to the formation of oxide products, are not consistent with our XRD results. At 600 °C, very small and broad 200_{MgO}, 111_{CaO}, and 220_{CaO} Bragg peaks appeared (Fig. 2a). At this *T* the degree of conversion α was 0.05 ($\alpha = M_0 - M_T/M_F$, being M_0 the mass of dolomite at the beginning of the experiment, M_T the mass at a given *T*, and M_F the mass at the end of the full decomposition). Failure to detect any product at a lower *T* (i.e., at lower α values) appears to be due to: (1) the dilution effect that grinding brings about, and (2) the possibility that nascent product oxides were poorly crystalline or even amorphous (Britton et al. 1951; Powell and Searcy 1978). The latter is consistent with the fact that, initially, lime and periclase Bragg peaks were very weak and broad, and subsequently underwent a clear sharpening and intensity increase with rising *T* (Fig. 2a). This is also in line with works reporting that: (1) lime and periclase Bragg peaks are first detected at a *T* about 100–200 °C higher than that corresponding to the onset of decomposition determined from TG and/or DTA (Engler et al. 1989), and (2) in situ XRD analyses showing a significant reduction in the intensity of dolomite peaks at a *T* ca. 200 °C lower than that corresponding to the first detection of product oxides (Readman and Blom 2005).

In the *T* range 650–750 °C, powder XRD showed a very broad, low-intensity peak that at the lowest *T* had a *d*-spacing of 3.005 Å and changed to 3.03 Å as *T* increased up to 750 °C. This peak corresponds to the 104 reflection of Mg-calcite [initially with ~9 mol% Mg, calculated according to Goldsmith and Graf (1958)], which became pure calcite with rising *T*. The formation of Mg-calcite is associated with mass effects contributing to an increase in pCO_2 within and around the sample, sufficient to induce the so-called "half decomposition" in air and resulting in the two-stage weight loss (Fig. 1). These results are in line with those of Lange and Roesky (1964), who report the formation of Mg-calcite in air, along with MgO and CaO, and conclude that it formed by recarbonation of (impure) CaO. Because pCO_2 was not sufficiently high, a fraction of CaO remained uncarbonated. In contrast, other authors (Hashimoto et al. 1980; Milodowski et al. 1989; De Aza et al. 2002; Galai et al. 2007) conclude that Mg-calcite forms directly from dolomite following its "half decomposition" in a CO_2 atmosphere However, as we will discuss later on, the direct formation of Mg-calcite is not consistent with our results.

XRD analyses of single-crystal pseudomorphs (run A) revealed no product phases at $T \leq 550$ °C. As in the case of powder samples, CaO and MgO Bragg peaks, although very broad and of very low intensity, were first detected at 600 °C (Fig. 2b). Because dolomite single crystals were oriented along the cleavage plane, no reflections other than $104_{dolomite}$ and $208_{dolomite}$ (that underwent a significant reduction in intensity) were present. Upon further heating up to 650 °C, lime and periclase Bragg peaks increased in intensity and were better defined. At 650 °C, the $104_{dolomite}$ peak was further reduced in intensity and a reflection at 3.01 Å corresponding to Mg-calcite with a ~8 mol% Mg appeared. Although very broad, it was better defined and more intense than that observed in ground samples (Fig. 2b). At $T >$ 750 °C, a continuous increase in the intensity and sharpening of lime and periclase Bragg peaks was observed. At 800 °C, dolomite fully disappeared. No traces of Mg-calcite (or calcite) were detected in single-crystal pseudomorphs calcined at $T \geq$ 750 °C. Apparently, Mg-calcite appeared as a transient phase on the surface of the pseudomorph and, as *T* increased, rapidly transformed into pure calcite, which later decomposed into CaO + CO_2. Such a compositional evolution can easily be explained by thermally activated Mg ions (with smaller radius than Ca ions) diffusion out of the calcite structure (Milodowski et al. 1989),

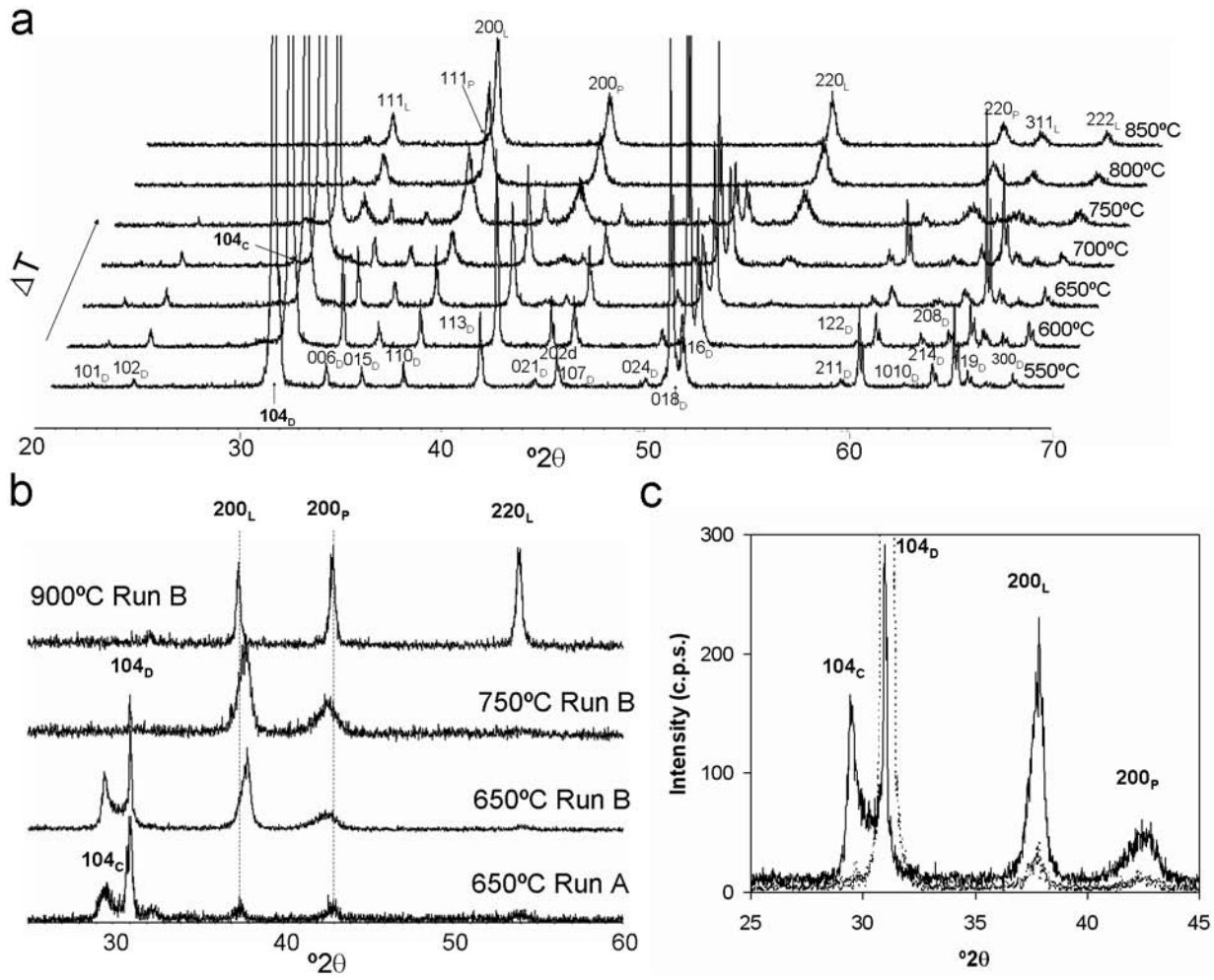

FIGURE 2. XRD diffraction patterns of: (**a**) powder samples of dolomite pseudomorphs calcined at different *T* in run A. *hkl* Bragg peaks are indicated for dolomite (subscript D), Mg-calcite (subscript C), lime (subscript L), and periclase (subscript P); (**b**) dolomite single-crystal pseudomorphs calcined at different *T* in runs A and B. Note the shifting of 200_{oxide} peaks of run B pseudomorphs from their theoretical position (dashed vertical lines); (**c**) detail of single-crystal pseudomorphs (run B) calcined for 5 min (dotted line pattern) and 15 min (solid line pattern). A well-formed Mg-calcite 104 Bragg peak only appears after 15 min calcination, while oxide 200 peaks are already present after only 5 min calcinations.

as demonstrated by Readman and Blom (2005).

The products crystallite size increased with *T* from 15–19 nm (750 °C) up to 36–44 nm (1000 °C) in the case of CaO and from 12–16 nm (750 °C) up to 38–44 nm (1000 °C) in the case of MgO. These results suggest that nascent CaO and MgO nanocrystals coarsened due to oriented aggregation and sintering, as it has been described for the case of CaO formed during the thermal decomposition of calcite (Rodriguez-Navarro et al. 2009). These results also show that there is no significant difference in crystallite size between CaO and MgO. Haul and Raal (1955) report a similar trend in the variation of crystallite size with *T*. However, their crystallite size values span from 9 nm (MgO) and 12 nm (CaO) at 750 °C, up to 100 nm at 1000 °C, possibly due to enhanced sintering in a CO_2 atmosphere. Note that enhanced sintering of product oxides has been associated to CO_2 (g) and H_2O (g) (Beruto et al. 2003a, 2003b).

In the case of run B, CaO and MgO Bragg peaks were first detected in single-crystal pseudomorphs calcined at 650 °C, i.e., at a *T* 50 °C higher than that at which they first appeared in run A. This is associated with the short soaking time during run B "flash" decomposition. Dolomite was present in all runs performed within 500–750 °C and disappeared at 800 °C (Fig. 2b). A well-defined 104 Bragg peak corresponding to Mg-calcite with ~5–7 mol% Mg was observed in samples calcined for 15 min at 650 °C (Fig. 2b). The fact that no Mg-calcite peak was observed in single-crystal pseudomorphs calcined at $T > 650$ °C (both in runs A and B) while such reflection was observed in ground samples calcined at a *T* up to 750 °C (run A) shows that this carbonate underwent a rapid decomposition once formed on the surface of the samples, and such a reaction front progressed toward the sample core. This is consistent with Britton et al. (1951) observation that the calcite layer formed upon half decomposition of dolomite lags the dolomite reaction front. Note that only the outer surface layer, ca. 100 nm in thickness, effectively

contributes to XRD when using low-penetrative Cu$K\alpha$ radiation.

Interestingly, "flash" decomposition at 650 °C with 5 or 10 min soaking time revealed either the absence of the $104_{Mg\text{-}calcite}$ Bragg peak or the presence of a extremely small $104_{Mg\text{-}calcite}$ peak, along with broad 200_{CaO} and 200_{MgO} peaks (Fig. 2c). A longer soaking time of 15 min resulted in a significant increase in the intensity of the $104_{Mg\text{-}calcite}$ peak as well as the 200_{CaO} and 200_{MgO} peaks (Fig. 2c). On the one hand, these results show that Mg-calcite development is favored by increasing soaking time (i.e., higher fractional decomposition) at a constant T. On the other hand, they show that the formation of both CaO and MgO precedes the formation of Mg-calcite. This latter phase thus appears to form following the recarbonation of nascent CaO crystals.

Pseudomorphs calcined at 550–800 °C showed a systematic shifting of the Bragg peaks of CaO and MgO (to higher and lower angles, respectively), a shifting that was more prominent in run B than in run A (Fig. 2b). These results show the existence of a (partial) solid solution between CaO and MgO (Spinolo and Anselmi-Tamburini 1989). In this respect, it is worth noting that the thermal decomposition of mixed metal carbonates has been proposed as an efficient route for the synthesis of complex metal oxides with a broad range of solid-solution compositions (Rao and Gopalakrishnan 1987). The mole percentage of each oxide in the solid solution was calculated by using the following equation

$$C_{ss} = 100\frac{\left|X_{\text{theor}} - X_{\text{exp}}\right|}{\Delta d_{hkl}} \quad (1)$$

where X_{theor} and X_{exp} are the theoretical and experimental d_{hkl}-spacing (in Å), respectively, of a given hkl_{CaO} or hkl_{MgO} peak and Δd_{hkl} the difference between the theoretical d_{hkl}-spacing of a given hkl_{CaO} and the corresponding hkl_{MgO}. Although peak broadness and irregularity in shape evolution with T led to some data scattering, a clear trend was observed in both runs A and B showing that each oxide became purer as T increased (Fig. 3). A similar behavior has been observed by Readman and Blom (2005). This T-dependent effect, as well as the lower cation substitution at any given T of run A pseudomorphs if compared with those of run B, can be explained considering that a high T and/or a longer soaking time facilitate the de-mixing of the initial mixed oxide via counter diffusion of Mg and Ca ions to produce pure CaO and MgO end-members. This is fully consistent with the observation that "flash" decomposition at 650–700 °C using a soaking time of 5 min resulted in the highest values of cation substitution: 9.5–11 mol% Mg in CaO and 5–7 mol% Ca in MgO. Regarding the differences in the kinetics of Mg and Ca diffusion out of the oxide solid solution, Fisler and Cygan (1999) show that high-T diffusion of Mg in Mg-doped calcite is faster than Ca due to the smaller radius of Mg (0.66 Å) if compared with Ca (0.99 Å). This explains why the higher initial amount of Mg in CaO is fully lost at the same T as it is lost the lower initial amount of Ca in MgO.

Spinolo and Anselmi-Tamburini (1989) report that the first stage of dolomite decomposition in vacuum involves the formation of a mixed Ca-Mg oxide with composition ca. $Ca_{0.5}Mg_{0.5}O$. This mixed oxide with rock-salt structure, i.e., face centered cubic (FCC), rapidly follows de-mixing, or more exactly spinodal decomposition, to form non-pure end-members CaOss and MgOss (ss = solid solution). The solid-solution composition is dictated by the spinodal curve in the CaO-MgO phase diagram. At the relevant T (650–750 °C), the maximum amount of Mg that can be incorporated into CaO is ca. 17 mol%, while the maximum amount of Ca that can be incorporated into MgO is ca. 9 mol% (Spinolo and Anselmi-Tamburini 1989), values that are consistent with those determined here.

Our XRD analyses failed to detect the initial $Mg_{0.5}Ca_{0.5}O$ phase reported by Spinolo and Anselmi-Tamburini (1989) and observed by Cater and Buseck (1985) forming in situ, in the TEM, under high-vacuum conditions. Apparently, in air or in a CO_2 atmosphere, where dolomite decomposition occurs at a higher T than in vacuum, the higher ion mobility may lead to the rapid disappearance of this metastable phase upon its transformation into CaOss and MgOss. This may help explain why no study has ever reported the presence of $Ca_{0.5}Mg_{0.5}O$ following the decomposition of dolomite in air or in CO_2 atmosphere.

Orientation relationships: 2D-XRD results

The limited degree of conversion at $T < 750$ °C did not enable the identification of any preferred orientation of the oxide product in pseudomorphs calcined at such a relatively low T. Conversely, pole figures of pseudomorphs calcined at 750 °C (both in runs A and B) show the existence of a strong preferred orientation between CaO and MgO crystals and the dolomite precursor (Fig. 4). Two sets of $\{100\}_{CaO}$ and $\{100\}_{MgO}$ planes were oriented nearly parallel (~12°) to $\{10\bar{1}4\}_{dolomite}$. Note that $(10\bar{1}4)_{dolomite}$ is the projection plane (Fig. 4a). The one set best defined (Set 1 in Figs. 4b and 4d) shows that $[100]_{CaO}$ and $[100]_{MgO}$ were parallel to $[841]_{dolomite}$ or equivalent $<\bar{4}41>_{dolomite}$. The other set (Set 2 in Figs. 4b and 4d), best defined in the case of MgO, was located at 180° from the previous one. It displayed the same parent/product orientation relationship of Set 1, but it corresponded to a section of the dolomite precursor twinned along the $(10\bar{1}\bar{2})$ plane following the dolomite $\{01\bar{1}2\}$ twin law (see scheme in Fig. 4a). Note that such a common dolomite deformation twinning is favored at high T (Barber and Wenk 1979), and most probably occurred

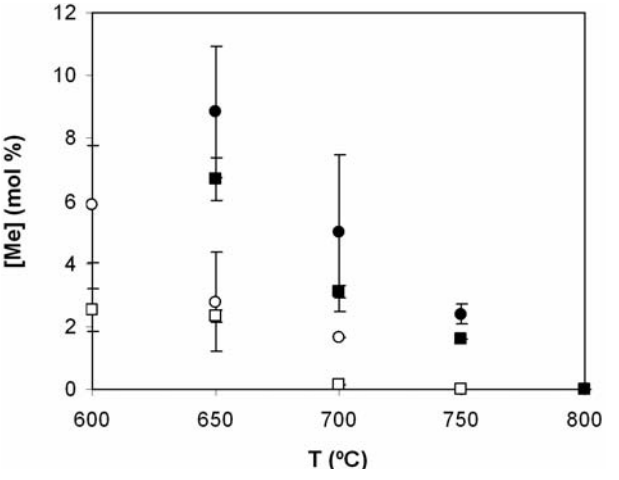

FIGURE 3. Variation of Me (Me = Mg or Ca) concentration in the product oxide solid solution with calcination T. Legend: solid symbols (run B), empty symbols (run A); circle = Mg in CaO; square = Ca in MgO.

during stress release associated to decrepitation. It resulted in sections of the precursor with $[841]_{dolomite}$ forming an angle of ca. 30° with $[841]_{dolomite}$ of the other sections of the twinned crystal, and oriented at 180°. The pole figures of $(220)_{CaO}$, $(111)_{CaO}$, $(220)_{MgO}$, and $(111)_{MgO}$ were consistent with the presence of two sets of CaO and MgO crystals, oriented with their [100] poles at ~30° with respect to each other. The pole figure of $(220)_{CaO}$ (Fig. 4c), as well as that of $(220)_{MgO}$, showed the following parent/product orientation relationships: $\{11\bar{2}0\}_{dolomite}//\{110\}_{oxide}$ and $\{11\bar{2}8\}_{dolomite}//\{110\}_{oxide}$. Figure 4e graphically depicts the observed orientation of Set 1 oxide product(s) with respect to the dolomite precursor (Fig. 4a). A 180° rotation of Figure 4e around an axis normal to the image plane yields the orientation of Set 2. Mg-calcite also showed a clear preferred orientation relationship with the dolomite precursor calcined at 750 °C (Fig. 4f). The following orientation relationships were observed: (1) $(10\bar{1}4)_{dolomite}$ nearly parallel to $(10\bar{1}4)_{Mg\text{-}calcite}$ and (2) $(11\bar{2}0)_{dolomite}//(11\bar{2}0)_{Mg\text{-}calcite}$. Interestingly, the orientation of Mg-calcite corresponded to that of the second subset of twinned dolomite, which is a subset with an orientation resulting from a 180° rotation of the dolomite crystal depicted in Figure 4a (corresponding to the orientation of the twin slab depicted in Fig. 4a). This suggests that the poorly defined orientation of $(200)_{CaO}$ of Set 2 (Fig. 4b) is due to a reduction in the 200 Bragg peak intensity of this set of CaO crystals after their (partial) recarbonation to yield Mg-calcite with a similar orientation as that of the precursor oxide. Pole figures of pseudomorphs calcined at 800, 900, and 1000 °C were very similar to those of 750 °C pseudomorphs. The only difference refers to the fact that high-*T* pseudomorphs presented two additional well-defined sets of $(200)_{CaO}$ pole maxima at 90° from each other, with two maxima at an angle of 30° (Set 3) and 60° (Set 4) with respect to the $(10\bar{1}4)_{dolomite}$ pole (Fig. 4g). This resulted in the appearance of an intense pole maxima corresponding to $(220)_{CaO}$, which was parallel to the pole of $(10\bar{1}4)_{dolomite}$ (Fig. 4h). These high-*T* orientation relationships were also present in pseudomorphs calcined at 750 °C, but they were not well defined (Figs. 4b and 4d). Such orientation relationships have been observed in the case of the thermal decomposition of calcite (Rodriguez-Navarro et al. 2009) and are consistent with XRD analyses of single-crystal pseudomorphs calcined at $T \geq 800$ °C, which showed that the 220_{CaO} Bragg peak was the most intense (Fig. 2b). These results suggest that the orientation relationships of Set 1 and Set 2 correspond to the initial stages of dolomite decomposition, while the orientation relationships of Set 3 and Set 4 correspond to the decomposition of Mg-calcite formed during the "half decomposition" of dolomite.

FESEM analysis of pseudomorphs

FESEM observations of the microtextural features of the pseudomorphs developed in run A gave, in general, a better picture of the calcination process and its evolution with *T* than those developed in run B. Therefore, we focus here on the results

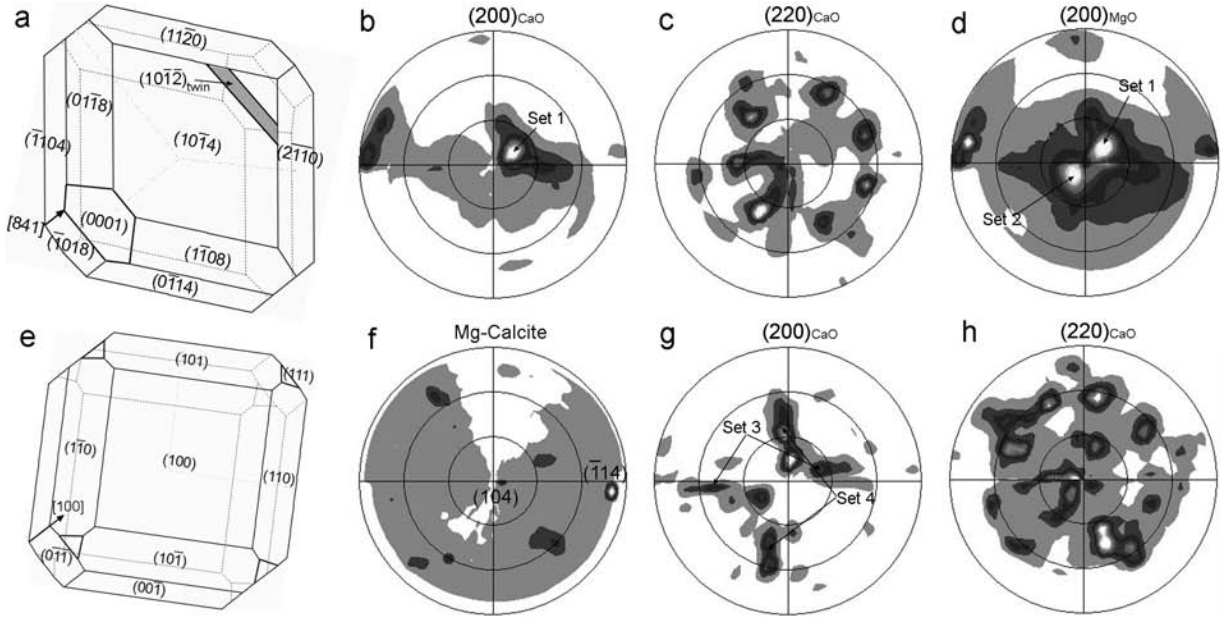

FIGURE 4. Pole figures of products formed upon thermal decomposition of dolomite single crystals: (**a**) scheme of dolomite rhombohedron resting flat on its $(10\bar{1}4)$ face (relevant crystal faces are depicted, as well as a slab, shaded corresponding to the $(10\bar{1}2)$ twin plane); (**b**) (200) and (**c**) (220) pole figures of CaO; (**d**) (200) pole figure of MgO. Note the existence of two sets (Sets 1 and 2) of CaO and MgO crystals with (100) planes forming an angle of ca. 12° with $(10\bar{1}4)_{dolomite}$ and with their poles rotated 180° with respect to each other, thus resulting in the two maxima in the (200) pole figures, best observed in (**d**). Set 1 displays the following orientation relationship: $[841]_{dolomite}//[100]_{oxide}$ and $\{11\bar{2}0\}//(110)_{oxide}$ as it is graphically displayed in the scheme of the oxide product (**e**). Set 2 displays an identical orientation relationship with respect to the twinned slab depicted in **a**; (**f**) (104) pole figure of Mg-calcite present at 750 °C, showing that the twinned slab in **a** shares the same orientation. At 1000 °C, the (200) pole figure of CaO (**e**) shows additional maxima corresponding to two sets of CaO crystals with (100) planes rotated ca. 90 ° (Sets 3 and 4) and forming and angle of 30° and 60° with respect to the [104] pole of dolomite. The corresponding (220) pole figure of CaO shows a maximum parallel to the (104) pole figure of the former Mg-calcite.

of the analysis of run A samples.

Textural changes associated with the decomposition of dolomite were clearly visible in samples fired at 600 °C. At this *T*, a highly porous aggregate of nanometer-sized (ca. 20–90 nm) anhedral crystals was observed on $(10\bar{1}4)_{dolomite}$ (Fig. 5a). These textural features were also observed in pseudomorphs fired at 650 and 700 °C. However, at these latter *T*, the development of cross-cutting cracks (Fig. 5b) and the growth of a subset of crystals (up to 100–400 nm in size) with better defined crystal faces (inset in Fig. 5b), were observed on the surface of the pseudomorphs. These larger crystals were more abundant under the surface layer, and displayed a highly oriented arrangement (Fig. 5c). They were lined by the nanocrystals shown in the inset of Figure 5a (i.e., MgO and CaO nanocrystals). These observations imply that: (1) either these larger crystals are CaO or MgO that underwent a very rapid oriented aggregation and coarsening (sintering) or (2) they are Mg-$CaCO_3$ crystals formed after the carbonation of (impure) CaO nanocrystals due to the build-up of CO_2 pressure as the calcination front moved toward the core of the dolomite crystal. The first hypothesis in not consistent with our XRD crystallite size measurements, which show nearly equal-sized CaO and MgO crystallites all along the calcinations process. Conversely, the second hypothesis is consistent with XRD results showing the formation of Mg-calcite in samples calcined at 650–700 °C. At 750–800 °C, massive, highly oriented cracks developed (Fig. 5d). Underneath these cracks the transformed rim was made up of highly oriented, elongated, blade-shaped crystals (Fig. 5e). The origin of the cracks appears to be related to the release of stress taking place once a sufficiently thick decomposed layer (ca. 50 μm thick) formed around the uncalcined core. Such a stress is built up due to molar volume differences between reactant and product phases (Beruto et al. 2004). Note that stress release is an important driving force in the decomposition of carbonates because it contributes to the diffusionless coarsening of oxide nanocrystals via an oriented attachment (Rodriguez-Navarro et al. 2009). Due to such an oriented attachment, the cracks display the observed well-defined orientation (Fig. 5d). Interestingly, the observed orientation relationships $\{11\bar{2}0\}_{dolomite}//\{110\}_{oxide}$ and $\{11\bar{2}8\}_{dolomite}//\{110\}_{oxide}$ suggest that the oxide crystals blades (Fig. 5e) are parallel to the cracks lips; that is they arrange with $[110]_{oxide}$ parallel to either $[010]_{dolomite}$ or $[2\bar{2}1]_{dolomite}$. At 750 °C, the transformed surface layer showed only one type of nanocrystals (ca. 50–100 nm in size) (inset in Fig. 5d). This textural change seems to be due to the surface decomposition of Mg-$CaCO_3$ crystals. Such a change is consistent with XRD results showing the absence of Mg-calcite on single-crystal pseudomorphs at 700–750 °C. However, such decomposition did not affected deeper layers at this *T*. At 800 °C, the reaction front was at a depth of ca. 100 μm, and at 850 °C, surface cracks were still clearly observed. At this latter *T*, the larger crystals lined by nanocrystals first observed on the surface of the pseudomorphs at 650 °C, and that disappeared from the outermost surface layer at 750 °C, also disappeared in the depth profile. They were replaced by a homogeneous highly porous aggregate of anhedral nanocrystals, ca. 50–100 nm in size, both at the surface of the pseudomorph (inset in Fig. 5f) and in the depth profile (Fig. 5f) (compare this texture with that depicted in Fig. 5c). As previously indicated, this textural change is due to the decomposition of Mg-$CaCO_3$ formed at lower *T*. This process is consistent with weight loss measurements and XRD results indicating that the plateau in the mass% vs. *T*, corresponding to the formation of Mg-$CaCO_3$, expanded from ~650 up to ~750 °C. Evidence for extensive sintering was observed at 900 °C. Interestingly, sintered crystals showed a highly oriented texture on the surface of the pseudomorph (Fig. 6a) consistent with the results of 2D-XRD analyses. The highest degree of sintering was observed at 1000 °C, where an oriented aggregate of micrometer-sized CaO and MgO crystals developed (Fig. 6b). Such a coarsening behavior has been extensively reported (e.g., Fonseca et al. 1998).

TEM analysis of pseudomorphs

Ex situ TEM observations failed to find any oxide product in pseudomorphs calcined at $T \leq 550$ °C (run A). This is possibly due to the difficulty in spotting a partially transformed area in samples with such a limited conversion ($\alpha \leq 0.02$). Pseudomorphs calcined at 600 °C showed the formation of scattered aggregates of oriented oxide nanocrystals (ca. 5–10 nm in size), typically at grain edges and/or lining fractures (Fig. 7a). At this relatively low *T*, however, we could not clearly identify which product phase was forming, because the SAED pattern only showed the spots corresponding to twinned dolomite (see the two sets of 110* and 018* reciprocal lattice vectors in inset of Fig. 7a), and a few diffuse halos corresponding to an unidentified poorly crystalline or nearly amorphous product(s). At 650 °C, it was clearly observed that the oxide nanocrystals formed a porous thin rim around the undecomposed dolomite core (Figs. 7b and 7c). Inset in Figure 7c shows the $[1\bar{1}0]$ zone-axis SAED pattern of dolomite, which also displays diffuse spots corresponding to $200_{(Ca,Mg)O}$. Such diffuse spots show that the oxide nanocrystals display a preferred orientation. The d_{200}-spacing of the oxide product is 2.15 Å, a value that according to Equation 1 corresponds to a mixed oxide with formula $Ca_{0.14}Mg_{0.86}O$. This shows that the degree of solid solution between MgO and CaO existing during the early stages of dolomite thermal decomposition is higher than that observed at higher *T* (XRD results). Some spots corresponding to a *d*-spacing of 2.98 Å were observed (inset in Fig. 7c). Such a *d*-spacing was assigned to the 104 reflection of Mg-calcite with a 16.8 mol% Mg content, a value higher than that determined from XRD. Such a discrepancy could in part be due to the error in determining *d*-spacings from SAED patterns. However, it is not ruled out the possibility that the initial (low-*T*) Mg-calcite may include a higher amount of Mg, which is ejected from the calcite structure as *T* and soaking time increase. It was observed that two sets of $[1\bar{1}0]_{dolomite}$ zone-axis SAED patterns overlapped (see reciprocal lattice vectors identified as 1* and 2* in inset of Fig. 7c). As in the case depicted in Figure 7a (inset), the overlapping of two reciprocal lattices is consistent with deformation twinning according to the $\{01\bar{1}2\}$ twin law, most probably induced by the thermal event. Such a twinning partially masked the orientation relationship(s) between parent and product phases. Nonetheless, the observed twinning explains why two sets (Set 1 and Set 2 in Fig. 4) of oriented oxide crystals were identified using 2D-XRD analysis.

Pseudomorphs calcined at temperatures ranging from 850 °C up to 950 °C showed oriented MgO and CaO crystals, which grew in size with calcination *T*. In some cases, the latter crystals

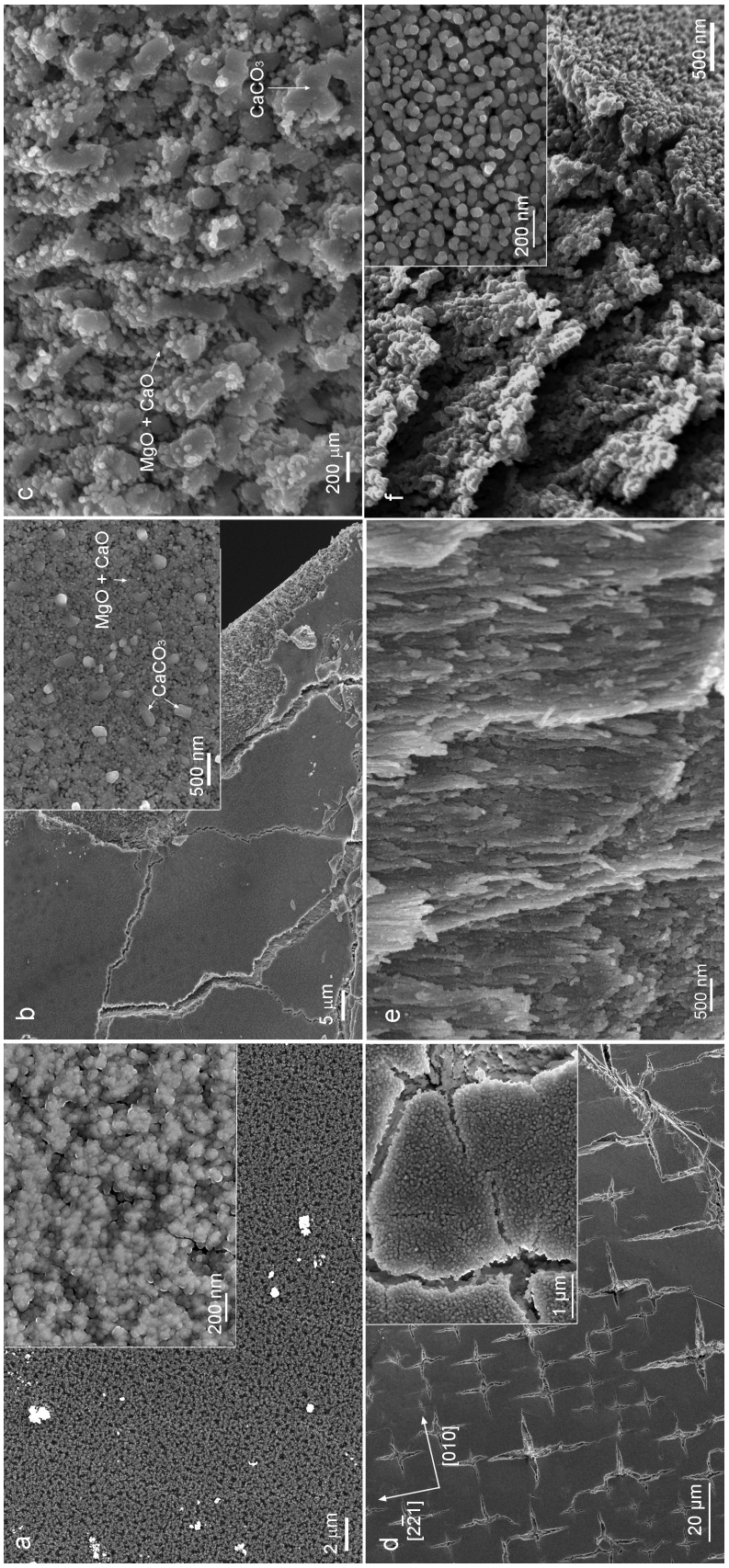

FIGURE 5. FESEM images of calcined dolomite pseudomorphs: (**a**) porous aggregate of oxide nanocrystals (see detail in inset) formed at 600 °C; (**b**) initial development of cross-cutting cracks at 700 °C and growth of a randomly distributed subset of Mg-calcite crystals up to 100–400 nm in size (inset); (**c**) detail of larger (0.2–1 μm in size), oriented calcite crystals surrounded by oxide nanocrystals underneath the surface of the pseudomorph at 700 °C; (**d**) oriented, star-shaped cracks formed at 750 °C (see detail in inset); (**e**) oriented blade-shaped crystals growing at 750 °C in a section normal to the dolomite pseudomorph cleavage plane; (**f**) porous aggregate of oxide nanocrystals formed at 850 °C after the decomposition of the carbonate (see detail in inset).

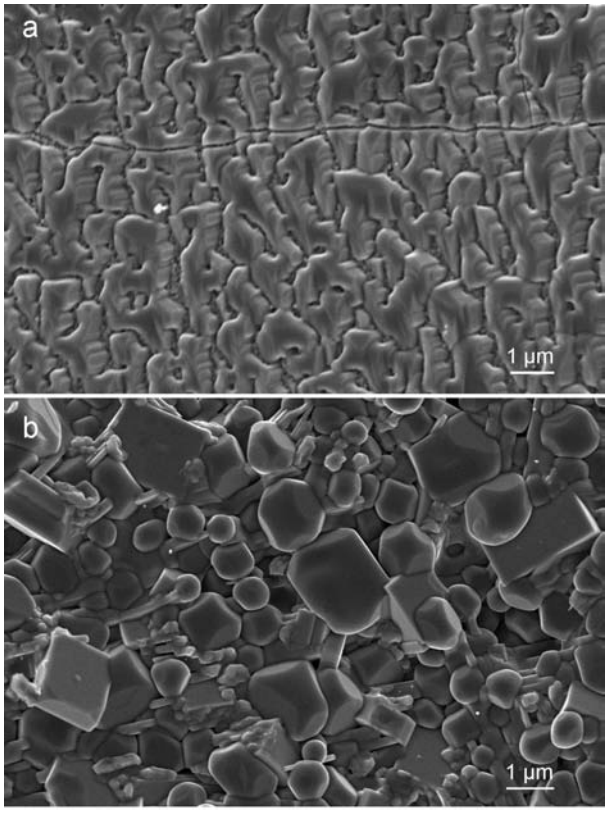

FIGURE 6. FESEM of dolomite pseudomorphs calcined in air: (**a**) oriented aggregate of oxide products showing sintering at 900 °C; (**b**) oxide crystals sintered at 1000 °C.

surrounded the former ones. These are typical features of sintered doloma (Fonseca et al. 1998). TEM observations confirm 2D-XRD and FESEM results regarding the existence of crystal coarsening via oriented aggregation and sintering, a coarsening that follows the same mechanistic path as that of CaO formed after calcite calcination (Rodriguez-Navarro et al. 2009).

In situ decomposition in the TEM

Decomposition of dolomite single crystals (ca. 2 to 5 µm in size) took place following exposure to the e-beam for about 1–5 min using a large condenser aperture (200 µm). No decomposition was observed (within a reasonable exposure time of up to 30 min) when using a small conderser aperture (100 µm). This experimental evidence demonstrates that the decomposition of dolomite by the e-beam is not principally due to direct bond-breaking (radiolysis), as suggested by Cater and Buseck (1985), which should be independent of the size of the condenser aperture at 200 kV. Rather, the effect appears to be primarily thermal as pointed out by Egerton and Malac (2004).

During the initial stages of decomposition, the pseudomorphs showed the typical mottled texture described by Wenk et al. (1983) resulting from beam damage (Fig. 8a). Upon full decomposition, the pseudomorphs were observed to be made up of a highly porous aggregate of two sets of oriented nanocrystals (crosscutting at 90°) with size ranging from 1 to 5 nm (Fig. 8b). Note that the theoretical porosity of fully decomposed dolomite is 55.2%. Interestingly, the products showed SAED patterns with large elliptical spots (Figs. 9 and 10) corresponding to a poorly crystalline, highly oriented aggregate of a single phase FCC oxide, similar to that described by Cater and Buseck (1985). The oxide showed the following d_{hkl}-spacings: $d_{111} = 2.63$; $d_{200} = 2.21$, and $d_{220} = 1.58$ Å. These d_{hkl}-spacings are intermediate between those of CaO ($d_{111} = 2.77$; $d_{200} = 2.40$, and $d_{220} = 1.70$ Å) and MgO ($d_{111} = 2.43$; $d_{200} = 2.10$, and $d_{220} = 1.49$ Å). The observed d_{hkl} values are consistent with a FCC mixed oxide with formula ~$Ca_{0.5}Mg_{0.5}O$. In one case, de-mixing of the oxide into two oxides (CaOss and MgOss) was observed upon long term exposure to the e-beam, thus resulting in the splitting of each single elliptical spot in the SAED pattern of the oriented oxide into two parallel elliptical spots (Fig. 11). The observed d_{hkl}-spacings indicate the formation of two oxide phases with formula $Ca_{0.75}Mg_{0.25}O$ and $Ca_{0.15}Mg_{0.85}O$. These compositions are consistent with those defined for the coherent spinodal curve in the system CaO-MgO (Spinolo and Anselmi-Tamburini 1989) and agree with that determined in pseudomorphs calcined in air at 650 °C.

SAED patterns showed two main orientation relationships between dolomite and the mixed-oxide product: (1) $[\bar{4}41]_{dolomite}$// $[100]_{oxide}$, with $(11\bar{2}0)_{dolomite}$//$(011)_{oxide}$, $(11\bar{2}8)_{dolomite}$//$(01\bar{1})_{oxide}$, and $(10\bar{1}4)_{dolomite}$^$(010)_{oxide}$~12° (Fig. 9); and (2) $[001]_{dolomite}$// $[1\bar{1}1]_{oxide}$ with $\{11\bar{2}0\}_{dolomite}$//$\{110\}_{oxide}$ (Fig. 10). These orientation relationships are fully consistent with those obtained by 2D-XRD analysis of dolomite pseudomorphs calcined in air. The second orientation relationship was also reported by Cater and Buseck (1985).

It is important to note that e-beam irradiation can lead to twinning and/or deformation resulting in the formation of carbonate subgrains with a different orientation. This is observed in Figure 10b where the development of a crack induces some missorientation in the product oxide crystals and results in additional, very weak (111) and (200) Debye rings. A similar effect is observed in Figure 11, where the $[001]_{dolomite}$ zone axis SAED pattern shows extra reflections (arrows in inset of Fig. 11a). As a consequence, the SAED pattern of the product oxide shows well-defined (very intense) spots corresponding to the $[1\bar{1}1]_{oxide}$ zone axis, plus additional (less intense) spots corresponding to 111 and 200 oxide reflections (inset in Fig. 11b). These effects may mask the existing crystallographic orientation relationship between reactant and product phases, as it has been described in the case of calcite (Rodriguez-Navarro et al. 2009).

The mechanism of thermal decomposition of dolomite

Our in situ TEM results are fully consistent with those of Cater and Buseck (1985) and Spinolo and Anselmi-Tamburini (1989) who observed the formation of a metastable FCC mixed oxide ($Mg_{0.5}Ca_{0.5}O$) following dolomite decomposition in vacuum. They are also consistent with the hypothesis presented by Britton et al. (1951) and Powell and Searcy (1978) on the existence of such a precursor of CaO and MgO. Spinolo and Anselmi-Tamburini (1989) have shown that this precursor oxide undergoes spinodal decomposition into impure CaO and MgO, as we have also observed here both in air and in vacuum (TEM). Our in situ TEM results corroborate those of Cater and Buseck (1985), who also observed the transformation of the mixed oxide into lime and periclase upon long-term exposure to the e-beam.

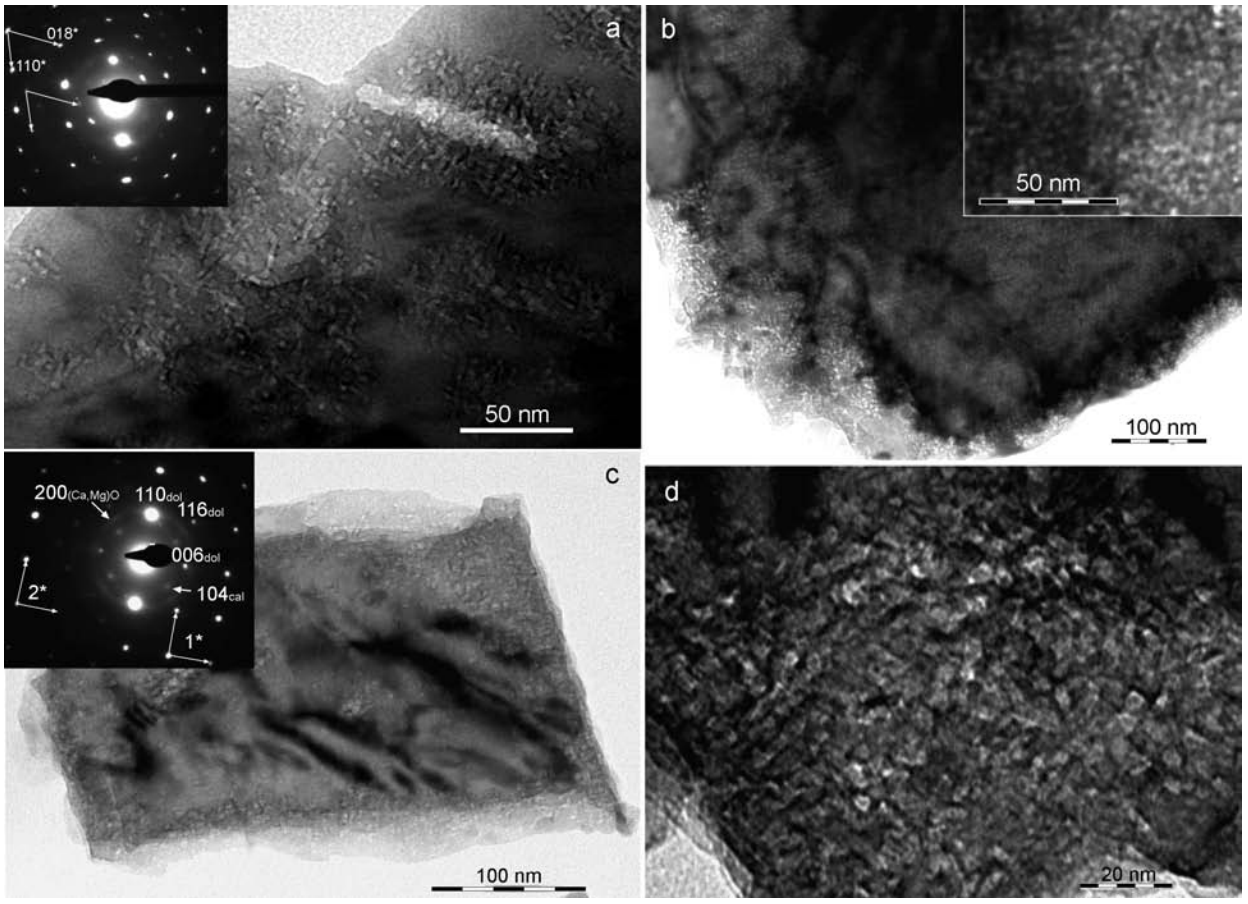

FIGURE 7. TEM images of dolomite pseudomorphs calcined in air: (**a**) initial decomposition at 600 °C resulting in the formation of oriented nanocrystals lining fractures. The [8$\bar{8}$1] zone axis of two reciprocal lattices corresponding to twinned dolomite is observed in the SAED pattern (inset); (**b**) porous pseudomorph formed at 650 °C where oxide product nanocrystals formed at the grain edges (see detail in inset); (**c**) pseudomorph partially transformed (at the edges) at 650 °C. It is twinned (see reciprocal vectors corresponding to two lattices, 1* and 2* in SAED pattern in inset) and shows diffraction spots corresponding to oriented (Ca,Mg)O and Mg-calcite (inset); (**d**) detail of oriented nanocrystals formed at the transformed edge of the pseudomorph in **c**.

However, these authors indicate that in one case such a transition occurred via the formation of an amorphous intermediate phase, which we have not observed. This is possibly due to the nature of the dolomite precursor used by Cater and Buseck (1985), which was made up of finely divided synthetic crystals 0.1 to 20 µm in size. Note that microcrystalline (ca. 1 µm grain size), disordered dolomite reportedly shows an unusual thermal decomposition behavior, including the formation of huntite [$CaMg_3(CO_3)_4$] plus Ca-rich dolomite as intermediate products (Navrotsky et al. 1999). Interestingly, we observe that the parent/product preferred crystallographic orientation is not lost at any stage of such a transformation; that is, during both thermal decomposition and spinodal demixing. This suggests that the formation of a purely amorphous phase during spinodal decomposition of the mixed oxide is highly improbable. If so, all crystallographic information should be lost during the formation of the amorphous phase. Conversely, the formation of a poorly crystalline intermediate phase (with short-range order) is not ruled out. Such a metastable phase may indeed evolve into crystalline, highly oriented product oxide(s) that can coarsen via an oriented aggregation mechanism (Penn and Banfield 1998). In this respect, the transformation of an amorphous phase displaying a short-range order into a crystalline phase, both sharing an intimate structural association, has been reported, for instance, in the case of the transformation of amorphous calcium carbonate (ACC) into a specific $CaCO_3$ polymorph (Lam et al. 2007).

Decomposition in air results in CaOss with up to 12 mol% Mg and MgOss with up to 8 mol% Ca as shown by our XRD analyses. However, the TEM-SAED analysis of pseudomorphs calcined at 650 °C shows the presence of mixed oxides with a higher degree of substitution. These results suggest that during the very early stages of dolomite decomposition in air, a precursor mixed oxide with similar stoichiometry as that observed during in situ decomposition in the TEM should have been formed. Nonetheless, the subsequent spinodal demixing erased any compositional evidence for its existence. We suggest that soaking time and increasing *T* are the triggering factors accounting for such a demixing and the subsequent formation of pure oxides that form via Ca and Mg diffusion out of periclase and lime, respectively. The fact that the initial mixed oxide is poorly

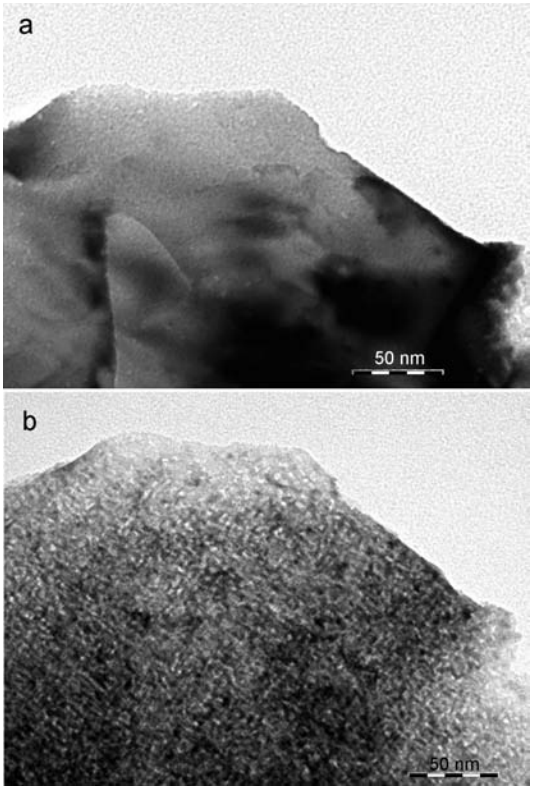

Figure 8. TEM photomicrographs of dolomite crystal: (**a**) at the beginning of e-beam irradiation and (**b**) after 5 min irradiation, resulting in full decomposition into a porous pseudomorph made up of oriented oxide nanocrystals.

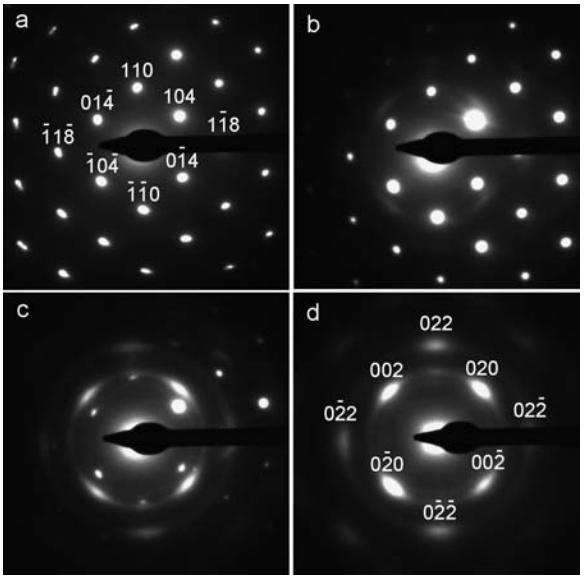

Figure 9. Sequence (**a**–**d**) of SAED patterns of dolomite (crystal depicted in Fig. 9) undergoing decomposition into (Ca,Mg)O: (**a**) dolomite [$\bar{4}$41] zone axis pattern before e-beam decomposition; (**b**) initial decomposition shown by the appearance of elliptical spots of the oxide; (**c**) further decomposition; and (**d**) complete transformation into oriented oxide crystals with their [100] zone axis parallel to dolomite [$\bar{4}$41].

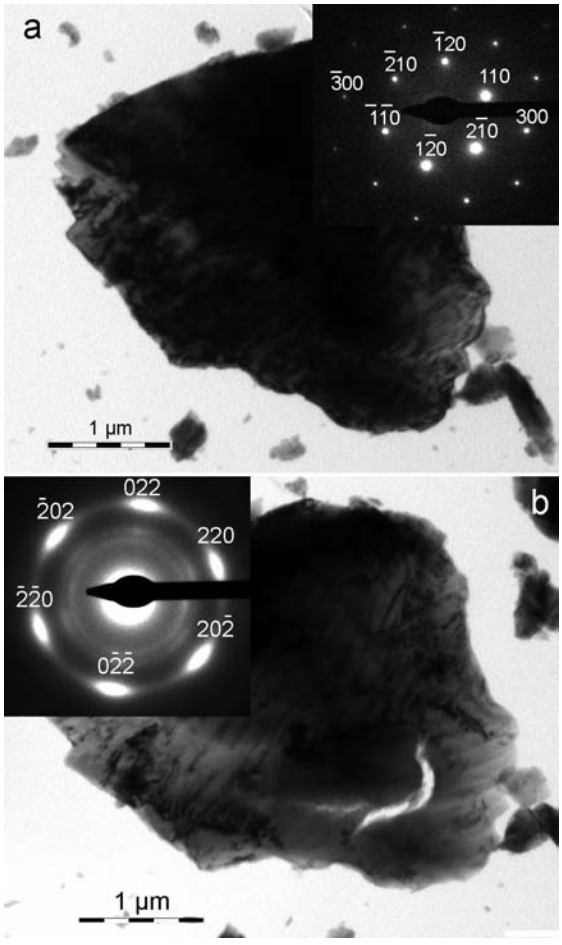

Figure 10. TEM photomicrographs of dolomite crystal. Part (**a**): before e-beam decomposition. The [001] zone axis SAED pattern of dolomite is shown in inset. Part (**b**): after 5 min e-beam irradiation, resulting in full decomposition into a porous pseudomorph made up of oriented oxide nanocrystals. The [1$\bar{1}$1] zone axis SAED pattern of the oxide is shown in inset. Additional, weak Debye rings corresponding 111 and 200 oxide reflections are also observed (see text for details).

crystalline may help explaining why we failed to identify it in the *T* range 500–600 °C when no product oxides were detected with XRD despite the fact that α reached a value of up to 0.05. Note that several authors have pointed out this fact as an oddity, which is that no products were observed during the early stages of dolomite decomposition. For instance, the NMR study by MacKenzie and Meinhold (1993) showed the presence of a magnesium oxide phase at a *T* when no oxide was detected by XRD. The authors conclude that this was "amorphous or poorly crystalline" MgO. However, the authors neglected the fate of Ca. Our results, and those of the authors reported above, suggest that in fact this oxide should correspond to a mixed oxide ($Mg_{0.5}Ca_{0.5}O$). Once the spinodal separation takes place, the oxide products (with limited solid solution) could be detected by XRD. With increasing *T* and time, the oxides become purer as confirmed by our XRD results.

Dolomite decomposition in high vacuum (in situ TEM) and in air results in oxide crystals that share a well-defined pre-

ferred crystallographic orientation with respect to the carbonate precursor. Such a crystallographic orientation is identical in pseudomorphs formed in air and in high vacuum. The observed preferred crystallographic orientation indicates that the decomposition of dolomite into the product oxides is topotactic, meaning that there is a 3D structural relationship between the carbonate and the product oxides. A close inspection of the structure of dolomite [$R\bar{3}$, hexagonal unit cell: a = 4.8079 and c = 16.010 Å (Lippmann 1973)] and that of a FCC oxide (either lime or periclase, or a FCC mixed oxide) shows that the alternating layers of metal and carbonate ions along the **c**-axis of dolomite match the configuration of alternating metal and oxygen layer along the <111> directions of the FCC oxide (Figs. 12a and 12c). The carbonate to oxide transformation involves the loss of CO_2 from the CO_3^{2-} groups, leaving O^{2-} that subsequently bond to the metal ions (Ca or Mg). Such a transformation requires shrinking along the carbonate **c**-axis, thus resulting in the observed (2D-XRD and SAED) 12° tilting of the former {10$\bar{1}$4} dolomite planes to form the {100} oxide planes. The structural similarity between those planes is clearly shown in Figures 12b and 12d: by loss of CO_2 from each CO_3^{2-} group, followed by bond shrinking, the (10$\bar{1}$4) dolomite plane easily transforms into the (100) oxide plane. Such a shear transformation occurs by diffusionless, limited, and cooperative ion displacement (Bertrand 1978). Due to the molar volume differences between the reactant and product phases, the continuity along specific crystallographic directions is lost, resulting in the formation of the highly oriented porous aggregates of nanocrystals observed here in pseudomorphs calcined in air and decomposed in situ following e-beam irradiation. Because the decomposition begins at a relatively low T of ca. 500 °C in air, or even lower in vacuum (decomposition in the TEM), Ca and Mg diffusion is hampered. As a consequence, the alternating Ca and Mg layers in dolomite are "frozen" as the newly formed mixed oxide crystallizes. However, further heating results in demixing (spinodal decomposition) and purification of each individual oxide via diffusion as T rises. All in all, the topotactic relationship between dolomite and each individual product oxide is preserved during every stage of the transformation both in vacuum and in air. In contrast to what was stated by Haul's group, and believed by numerous authors, these results confirm that the thermal decomposition of dolomite follows the same mechanistic path regardless the value of pCO_2.

It should be noted that the thermal decomposition of other carbonates such as calcite (Rodriguez-Navarro et al. 2009), siderite $FeCO_3$ (Dasgupta 1961), magnesite $MgCO_3$ (Singh Dev 1972), and otavite $CdCO_3$ (Floquet and Niepce 1978) has been shown to be topotactic. Interestingly, the parent-product orientation relationship in dolomite is simpler than that observed in the

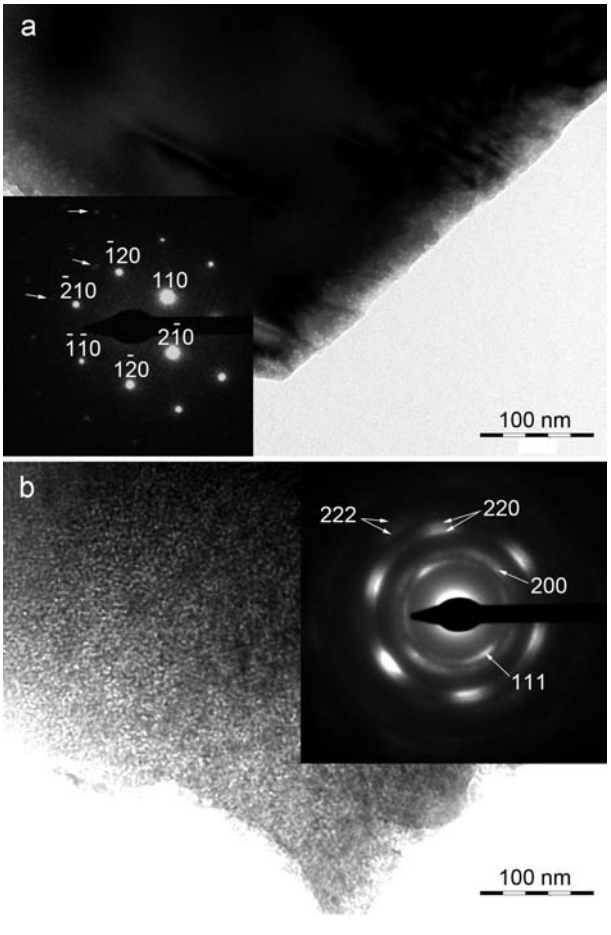

FIGURE 11. TEM photomicrographs of dolomite crystal. Part (**a**): at the beginning of e-beam irradiation. The [001] dolomite zone axis SAED pattern (inset) shows extra spots (arrows) corresponding to the reciprocal lattice of a twinned section. Part (**b**): after 5 min irradiation, resulting in full decomposition into a porous pseudomorph made up of oriented oxide nanocrystals. The [1$\bar{1}$1] oxide zone axis SAED pattern shows split spots due to demixing of (Ca,Mg)O. Extra 111 and 200 reflections (also showing splitting) are observed (see text for details).

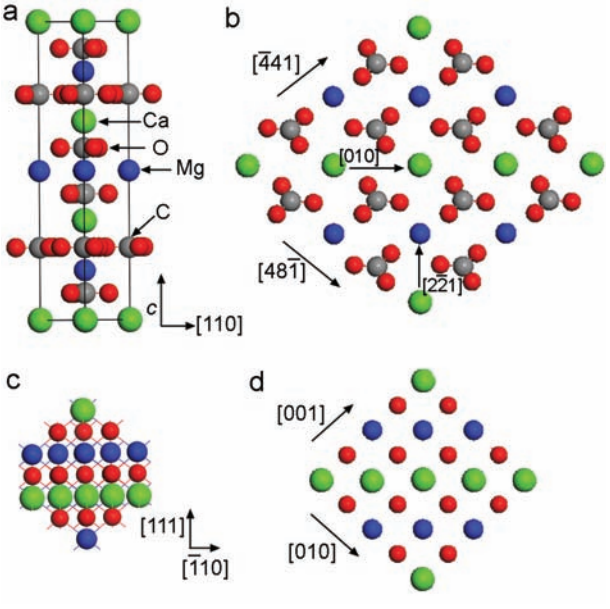

FIGURE 12. Scheme representing the structure of dolomite hexagonal unit cell (**a**), the projection of dolomite structure on the (10$\bar{1}$4) plane (**b**), the (ideal) structure of $Ca_{0.5}Mg_{0.5}O$ viewed along [$\bar{1}\bar{1}$2] (**c**), and the projection of the mixed oxide structure along [100] (**d**). (Color online.)

case of calcite, or other calcite-type carbonates such as otavite. This may be explained considering that calcite-type carbonates have a $R\bar{3}c$ structure, while the presence of alternating layers of Mg and Ca in dolomite, as well as the rotation of the carbonate groups around the **c**-axis, result in a symmetry reduction (space group $R\bar{3}$). This leads to the disappearance of the glide planes parallel to the **c**-axis and a reduction of the number of equivalent directions along which the oxide product can form during a topotactic transformation.

Another important finding refers to the formation of oriented Mg-calcite nanocrystals, which become pure calcite as *T* rises. Our XRD and FESEM results show that during the so-called "half decomposition" of dolomite in air, oriented Mg-calcite nanocrystals develop *after* the formation of CaOss and MgOss not *before*. It follows that Mg-calcite should have formed by solid-state reaction of CO_2 with the nascent CaOss nanocrystals. Such a reaction preserved the orientation of CaOss and led to the incorporation of Mg (present in CaOss) into the Mg-calcite structure. Note that the solid state (re)carbonation of CaO (i.e., "back-reaction") at the relevant *T* of our decomposition experiments has been extensively reported (Agrinier et al. 2001). Conversely, "back-reaction" experiments using thermally decomposed dolomite and magnesite detected no sign of (re)carbonation in the case of MgO (Agrinier et al. 2001), an observation consistent with our results. Once Mg diffuses out of Mg-calcite, the resulting calcite decomposes into CaO plus CO_2 at $T > 750$ °C. The parent calcite and the product CaO display the topotactic relationship determined by Rodriguez-Navarro et al. (2009).

Our results demonstrate that the so-called "half decomposition" or "half calcination" of dolomite bears no mechanistic significance. In fact, these terms are misleading, as they imply that a (hypothetical) $MgCO_3$ pseudophase in dolomite is first decomposed, leaving the other half of dolomite, which is the (hypothetical) $CaCO_3$ pseudophase, undecomposed when calcination begins in air or in a CO_2 atmosphere. We therefore suggest that the usage of such a misleading terminology should be discouraged, as there is no such thing as "half calcination" or "half decomposition", but rather a direct decomposition into the product oxides in one single stage, and subsequent CaOss recarbonation to form (Mg) calcite.

Acknowledgments

This work has been financially supported by the Ministerio de Educación y Ciencia, Spain, under Contract MAT2006-00578 and by EU Initial Training Network Delta-Min (Mechanisms of Mineral Replacement Reactions) grant PITN-GA-2008-215360. Financial support has also been provided by the research group RNM-179 (Junta de Andalucía, Spain). We thank the personnel of the Centro de Instrumentación Científica of the Universidad de Granada for assistance during TGA, 2D-XRD, TEM, and FESEM analyses. We thank D. Beruto for helpful discussion and for suggesting the flash decomposition experiments. We also thank A. Arizzi for her assistance during calcinations experiments and A. Rodriguez-Navarro for his help during 2D-XRD analyses.

References cited

Agrinier, P., Deutsch, A., Schärer, V., and Martinez, I. (2001) Fast back-reactions of shock-released CO_2 from carbonates: An experimental approach. Geochimica et Cosmochimica Acta, 65, 2615–2632.

Bandi, W.R. and Krapf, G. (1976) The effect of CO_2 pressure and alkali salt on the mechanism of decomposition of dolomite. Thermochimica Acta, 14, 221–243.

Barber, D.J. and Wenk, H.R. (1979) Deformation twinning in calcite, dolomite and other rhombohedral carbonates. Physics and Chemistry of Minerals, 5, 141–165.

Bertrand, G. (1978) Comments on "Kinetics of endothermic decomposition reactions. 2. Effect of the solid and gaseous product." Journal of Physical Chemistry, 82, 2536–2537.

Beruto, D.T., Vecchiattini, R., and Giordani, M. (2003a) Effect of mixtures of H_2O (g) and CO_2 (g) on the thermal half decomposition of dolomite natural natural stone in high CO_2 pressure regime. Thermochimica Acta, 405, 25–33.

——— (2003b) Solid products and rate-limiting step in the thermal half decomposition of natural dolomite in a CO_2 (g) atmosphere. Thermochimica Acta, 405, 183–194.

Beruto, D., Searcy, A.W., and Kim, M.G. (2004) Microstructure, kinetic, structure, thermodynamic analysis for calcite decomposition: Free-surface and powder bed experiments. Thermochimica Acta, 424, 99–109.

Best, M.G. (1982) Igneous and Metamorphic Petrology. Freeman, New York.

Bradley, W.F., Burst, J.F., and Graf, D.L. (1953) The crystal chemistry and differential thermal effects of dolomite. American Mineralogist, 38, 207–217.

Britton, H.T.S., Gregg, S.J., and Winsor, G.W. (1951) The calcinations of dolomite. Part II.-The Thermal decomposition of dolomite. Transactions of the Faraday Society, 48, 70–75.

Cater, E.D. and Buseck, P.E. (1985) Mechanism of decomposition of dolomite, $Ca_{0.5}Mg_{0.5}CO_3$, in the electron microscope. Ultramicroscopy, 18, 241–252.

Cultrone, G., Arizzi, A., Sebastián, E., and Rodriguez-Navarro, C. (2008) Sulfation of calcitic and dolomitic lime mortars in the presence of diesel particulate matter. Environmental Geology, 56, 741–752.

Dasgupta, D.R. (1961) Topotactic transformations in iron oxides and oxyhydroxides. Indian Journal of Physics, 35, 401–419.

——— (1967) Thermal decomposition of dolomite and ankerite. Mineralogical Magazine, 36, 138–141.

De Aza, A.H., Rodríguez, M.A., Rodríguez, J.L., De Aza, S., Pena, P., Convert, P., Hansen, T., and Turrillas, X. (2002) Decomposition of dolomite monitored by neutron thermodiffractometry. Journal of the American Ceramic Society, 85, 881–888.

Egerton, R.F. and Malac, P.L.M. (2004) Radiation damage in the TEM and SEM. Micron, 35, 399–409.

Engler, P., Santana, M.W., Mittleman, M.L., and Balazs, D. (1989) Non-isothermal, in situ XRD analysis of dolomite decomposition. Thermochimica Acta, 140, 67–76.

Fisler, D.K. and Cygan, R.T. (1999) Diffusion of Ca and Mg in calcite. American Mineralogist, 84, 1392–1399.

Floquet, N. and Niepce, J.C. (1978) Threefold transformation twin in the topotactic decomposition of cadmium carbonate crystals. Journal of Materials Science, 13, 766–776.

Fonseca, A.T., Vieira, J.M., and Baptista, J.L. (1998) Grain growth in synthetic and natural dolomas. Ceramics International, 24, 163–173.

Galai, H., Pijolat, M., Nahdi, K., and Trabelsi-Ayadi, M. (2007) Mechanism of growth of MgO and $CaCO_3$ during a dolomite partial decomposition. Solid State Ionics, 178, 1039–1047.

Galwey, A.K. and Brown, M.E. (1999) Thermal Decomposition of Ionic Solids. Elsevier, Amsterdam.

Goldsmith, J.R. and Graf, D.L. (1958) Relation between lattice constant and composition of the Ca-Mg carbonates. American Mineralogist, 43, 84–101.

Grapes, R. (2006) Pyrometamorphism. Springer, Berlin.

Hashimoto, H., Komaki, E., Hayashi, F., and Uematsu, T. (1980) Partial decomposition of dolomite in CO_2. Journal of Solid State Chemistry, 33, 181–188.

Haul, R.A.W. and Markus, J. (1952) On the thermal decomposition of dolomite. IV. Thermogravimetric investigation of the dolomite decomposition. Journal of Applied Chemistry, 2, 298–306.

Haul, R.A.W. and Raal, F.A. (1955) Zur thermischen Zersetzung von Dolomit. VI. Adsorptionsuntersuchungen an thermisch zersetzten Dolomitkristallen. Zeitschrift für Anorganische und Allgemeine Chemie, 281, 199–211.

Lam, R.S.K., Charnock, J.M., Lennie, A., and Meldrum, F.C. (2007) Synthesis-dependent structural variations in amorphous calcium carbonate. Crystal Engineering Communications, 9, 1226–1236.

Lange, P.A. and Roesky, H. (1964) Untersuchungen zur thermischen Dissoziation von Dolomit. Berichte Deutsche Keramik Gesellschaft, 41, 497–499.

Lippmann, F. (1973) Sedimentary Carbonate Minerals. Springer-Verlag, Berlin.

MacKenzie, K.J.D. and Meinhold, R.H. (1993) Thermal decomposition of dolomite (calcium magnesium carbonate) studied by ^{25}Mg solid-state nuclear magnetic resonance. Thermochimica Acta, 230, 331–337.

McCauley, R.A. and Johnson, L.A. (1991) Decrepitation and thermal decomposition of dolomite. Thermochimica Acta, 185, 271–282.

Milodowski, A.E., Morgan, D.J., and Warne, S.St.J. (1989) Thermal analysis studies of the dolomite-ferroan dolomite-ankerite series. II. Decomposition mechanism in flowing CO_2 atmosphere. Thermochimica Acta, 152, 279–297.

Navrotsky, A., Doodley, D., Reeder, R., and Brady, P. (1999) Calorimetric studies of the energetics of order-disorder in the system $Mg_{1-x}Fe_xCa(CO_3)_2$. American Mineralogist, 84, 1622–1626.

Penn, R.L. and Banfield, J.F. (1998) Imperfect oriented attachment: Dislocation generation in defect-free nanocrystals. Science, 281, 969–971.

Powell, E.K. and Searcy, A.W. (1978) Kinetics and thermodynamics of decom-

position of dolomite to a metastable solid product. Journal of the American Ceramic Society, 61, 216–221.
Rao, C.N.R. and Gopalakrishnan, J. (1987) Synthesis of complex metal oxides by novel routes. Accounts of Chemical Research, 20, 228–235.
Readman, J.E. and Blom, R. (2005) The use of in-situ powder X-ray diffraction in the investigation of dolomite as a potential reversible high-temperature CO_2 adsorbent. Physical Chemistry Chemical Physics, 7, 1214–1219.
Rodriguez-Navarro, C., Ruiz-Agudo, E., Luque, A., Rodriguez-Navarro, A.B., and Ortega-Huertas, M. (2009) Thermal decomposition of calcite: Mechanisms of formation and textural evolution of CaO nanocrystals. American Mineralogist, 94, 578–593.
Samtani, M., Dollimore, D., Wilburn, F.W., and Alexander, K. (2001) Isolation and identification of the intermediate and final products in the decomposition of dolomite in an atmosphere of carbon dioxide. Thermochimica Acta, 367– 368, 285–295.
Siegel, S., Fuchs, L.H., Hubble, B.R., and Nielsen, E.K. (1978) Relationship between the morphological properties of half-calcined dolomite and the kinetics of the sulfation reaction. Environmental Science and Technology, 12, 1411–1416.
Singh Dev, R. (1972) Topotaktische Phänomene bei der Calcinierung, Sulfatisierung und Chloridisierung einiger Karbonat-Einkristalle. Neues Jahrbuch für Mineralogie, Monatshefte, 1, 12–22.
Spinolo, G. and Anselmi-Tamburini, U. (1989) Nonequilibrium (Ca,Mg)O solid solutions produced by chemical decomposition. Journal of Physical Chemistry, 93, 6837–6843.
Wenk, H.R., Barber, D.J., and Reeder, R.J. (1983) Microstructures in carbonates. In R.J. Reeder, Ed., Carbonates: Mineralogy and Chemistry, 11, p. 301–367. Reviews in Mineralogy, Mineralogical Society of America, Chantilly, Virginia.
Wiedemann, H.G. and Bayer, G. (1987) Note on the thermal decomposition of dolomite. Thermochimica Acta, 121, 479–485.
Wilsdorf, H.G.F. and Haul, R.A.W. (1951) X-ray study of the thermal decomposition of dolomite. Nature, 167, 945–946.

Manuscript received February 21, 2011
Manuscript accepted August 13, 2011
Manuscript handled by Matthias Gottschalk